Effects of Material and Treatment Parameters on Noise-Control Performance of Compressed Three-Layered Multifiber Needle-Punched Nonwovens

Nazire Deniz Yilmaz,[1] Stephen Michielsen,[2] Pamela Banks-Lee,[2] Nancy B. Powell[2]

[1]Department of Textile Engineering, Pamukkale University, Denizli 20020, Turkey
[2]College of Textiles, North Carolina State University, Raleigh, North Carolina 27695

ABSTRACT: The effects of material and treatment parameters on airflow resistivity and normal-incidence sound absorption coefficient (NAC) of compressed three-layer nonwoven composites have been studied. Material parameters included fiber size and porosity, and treatment factors included applied pressure and duration of compression. Fibers used included poly(lactic acid) (PLA), polypropylene (PP), glassfiber, and hemp. Three-layered nonwoven composites were classified based on material content and fiber blend. LHL and PGP were sandwiched structures consisting of PLA/Hemp/PLA and PP/glassfiber/PP layers, respectively. PGI consisted of three layers of an intimate blend of PP and glassfiber. Statistical models were developed to predict air flow resistivity from material parameters and the change in air flow resistivity from compression parameters. Independent variables in the first model were porosity and fiber size and, in the latter model, were compressibility, pressure, and initial material parameters. An increase in air flow resistivity was found with increased compression. No significant effect of compression duration was detected. Two additional statistical models were developed for the prediction of sound absorption coefficient based on material and treatment parameters. The independent variables of the first model were air flow resistivity, thickness, and frequency, and those of the second model were compressibility, initial thickness, and initial density of the composite, diameter and density of the fiber, compression pressure, and frequency. A decrease in sound absorption coefficient was detected with increasing compression, while no effect of duration was detected. © 2011 Wiley Periodicals, Inc. J Appl Polym Sci 123: 2095–2106, 2012

Key words: sound absorption; compression; nonwoven; layered composites; biodegradable

INTRODUCTION

There is an ever increasing demand for better living and working environments.[1] To meet this demand, noise reduction is a must; as noise has negative effects on physiological and psychological human health, besides deteriorating working and learning efficiencies.[2] This situation makes noise control engineering more important and more complicated, taking diversified life styles into consideration.[1]

Noise control can be achieved by three means. Primary methods include alterations at noise and vibration sources. Secondary methods include modifications along the sound propagation path, and tertiary methods deal with sound receivers. Primary methods are constrained by technical and economical parameters; while tertiary methods necessitate that each receiving person is treated individually. This makes the secondary methods, which include the uses of sound barrier and absorbers, relatively practical and cost-efficient.[2,3]

Sound absorbers are porous materials that can be classified into three groups: cellular materials like foams, granular materials like woodchip panels, and fibrous materials like nonwoven stuctures.[3] Sound dissipation occurs in the tortuous pore channels of porous materials due to viscosity and heat conductivity of the medium.[4,5]

Among fibrous materials, nonwovens are promising materials for noise reduction applications. Compared to foams, nonwovens are advantageous in that they absorb more sound over a broader frequency range.[6] Also, nonwovens can be recycled and may have more environmentally friendly manufacturing methods compared to polyurethane foams.[7]

In studying acoustic properties of porous materials, acoustic impedance, Z, is a very important material characteristic. Acoustical impedance, defined by eq. (1), is the ratio between the sound pressure, p, and the particle vibration velocity, v_x[1,3]:

$$\frac{p}{v_x} = -Z. \tag{1}$$

Acoustical impedance is the most important feature of a material in terms of its acoustical properties.[3] As seen from eqs. (2) and (3), acoustical impedance determines the absorption performance of the porous material.

$$Я = \frac{Z_1 - Z_0}{Z_1 + Z_0}, \tag{2}$$

where $Я$ is the reflection coefficient, Z_0 is the acoustical impedance of free air, and Z_1 is the acoustical surface impedance of the porous material.[1]

$$\alpha_n = 1 - |Я|^2 \tag{3}$$

where α_n is the normal incident sound absorption coefficient.

Equation (2) shows that when the difference between the acoustical impedances of air and porous material increases, more sound will be reflected back from the surface of the material. From eq. (3), it is clear that the more incident sound that is reflected, the less sound energy that is available to be absorbed.[8] The acoustical impedance is composed of two components, resistance and reactance as shown in eq. (4):

$$Z = R + i\chi, \tag{4}$$

where Z is the impedance, R is the resistance, which is a real quantity, and χ is the reactance, which is imaginary.[9]

Air flow resistance, R, given in eq. (4), is among the main parameters that determine sound absorption. Air flow resistivity, r_0, which is air flow resistance corrected by the surface area and the thickness of porous material is an intrinsic feature of porous materials. A number of researchers have used air flow resistivity to model sound absorption.[10–13] Air flow resistivity is given by eq. (5),

$$r_0 = \frac{p \cdot S}{l \cdot u}, \tag{5}$$

where r_0 is the flow resistivity, in mks rayl/m (Pa s m^{-2}), p is pressure in Pa, S is the sample area, in square meter, l is the thickness of the porous material in meter, and u is the volumetric velocity of the fluid in cubic meter per second.[14]

Air flow resistivity is important for a number of applications including noise control,[2] filtration,[15] barrier,[16] and comfort.[17] In fibrous materials, flow resistivity increases with decreasing fiber diameter. Other than fiber size, fabric density, porosity, tortu-

osity,[18] mean pore size, pore size distribution,[15] fiber orientation,[12] and fabric surface characteristics[19] also affect flow resistivity.

Compression molding, a commonly used method in the plastics industry, is widely used in automotive production to manufacture large parts. Because of its simplicity and low amount of waste, it is a cost-efficient process.[8] Compression molding also has wide use in converting planar nonwoven fabrics to 3-D structures.[2] This makes it necessary to study the effects of compression molding on the performance of such sound absorbers.

The compression-molding process has two components: compression and heating.[2] Limited research effort has been devoted to investigating the effect of compression on the sound absorption performance of nonwovens. Castagnede et al.[20] found a decrease in sound absorption in a fibrous mat due to compression. Compression led to a decrease in porosity and thickness, and an increase in tortuosity and resistivity. Similarly, a decrease in sound absorption with compression was also reported by Jayaraman et al.[21]

In this work, air flow resistivity and sound absorption properties of compressed three-layered multifiber nonwoven composites, which included conventional fibers such as polypropylene (PP) and glassfiber, an engineered biodegradable fiber, poly (lactic acid) (PLA), and hemp, a natural fiber, were studied. The effects of material and treatment factors on noise control performance of compressed nonwoven composites were investigated. The effect of heating during compression molding was not addressed in this work.

EXPERIMENTAL

Materials

Four fiber types were used in production of nonwoven samples: PP, PLA, glassfiber, and hemp. PP fibers, PLA fibers, and cardable glassfibers were donated by Nonwovens Cooperative Research Center (NC, USA), Fiber Innovation Technology (TN, USA), and AGY (SC, USA), respectively. Hemp fibers that were field retted and processed through BioFibeRefinery™ were purchased from Stemergy (Canada, Ontario). PP and glassfibers were selected due to the fact that these fiber types are commonly used in conventional nonwoven composites as the carrier and reinforcement materials, respectively.[13] PLA was selected as a biodegradable alternative carrier fiber. Hemp was selected as the natural biodegradable reinforcement fiber as its mechanical properties are comparable to those of flax.[13] Properties of the fibers are given in Table I.

TABLE I
Fiber Parameters

| Fiber | Structure | Void ratio (%) | Fiber radius $\times 10^{-6}$ (m) | | Fiber density $\times 10^{-3}$ (kg m^{-3}) | Apparent fiber density $\times 10^{-3}$ (kg m^{-3}) |
			Mean	σ		
PLA	Hollow	18	30.9	3.1	1.24	1.02
PP	Solid	N.A.	31.7	1.3	0.91	0.91
Glassfiber[a]	Solid	N.A.	9.00	0.74	2.50	2.50
Glassfiber[b]	Solid	N.A.	10.9	0.82	2.50	2.50
Hemp	Multifibrillar	N.A.	42	38	1.45	1.45

[a] Glassfiber in layered PP/glassfiber/PP blend.
[b] In intimate polypropylene–glassfiber blend.

Sample preparation

Fibers went through three steps during nonwoven production: fiber opening, web formation, and web bonding. A Truetzschler® Opener was used to open the fibers that were supplied in dense press-packed bales. All fiber types were opened in monofiber form except for one sample set, which includes a blend of 33% glassfiber and 66% PP fiber.

For web forming, an air-laying method was used. In this method, fibers were fed into an air stream and then transferred to a perforated drum or moving belt where the fiber web was formed. Air laying was carried out in a Truetzschler® Tuft Feeder Scanfeed. The target basis weight was set at 330 g/m² (gsm). Table II shows the produced webs. After formation, webs were preneedled using a NSC Asselin® Preneedler.

Needle-punching, where the fibers were entangled by mechanical action, was used for web bonding. Before needle-punching, three layers of webs were stacked to form PGP, LHL, and PGI nonwoven structures as shown in Table III. Figure 1 gives a general production flow chart, in which layers A and B may or may not be the same fiber type.

A NSC Asselin needle-punch loom was used for bonding three-layered webs. The loom setting was 100 cm min^{-1} speed, 100-cm width, with needles on both sides, 228 strokes cm^{-1}, 175 punches cm^{-2} penetration density, and 3-mm penetration depth. Groz-Beckert® 15 × 17 × 40 × 3 needles were used. The target basis weight was set at 1000 gsm (g m^{-2}). Schematic diagrams of nonwoven fabrics produced using needle-punching are shown in Figure 2.

Compression

A Pasadena Hydraulics (P.H.I) model hydraulic press was used for this treatment. Level and duration of pressure were varied, while the temperature was set constant at room temperature. Compression conditions for LHL, PGP, and PGI are shown in Table IV. Because of limited availability of hemp fibers of the specific batch used, a reduced experimental set up was applied to LHL fabrics.

Characterization

Fibers were characterized based on their diameters. Fabrics were characterized in terms of mass per unit area, thickness, porosity, and air flow resistivity. Samples were subjected to conditioning in 20°C and 65% relative humidity for at least 24 h before characterization processes.

Fiber linear density

Average diameters of all fibers were determined according to ASTM D 1577-07 Standard Test Methods for Linear Density of Textile Fibers.[22] Average linear densities of the fibers were obtained by fiber diameter measurements on the scanning electron microscope images. A Hitachi® S-3200N Scanning Electron Microscope at the Analytical Instrumentation Facility of North Carolina State University was used. 4Pi EDS®/Digital Imaging system was used to

TABLE II
Fiber Webs Produced by Truetzschler
Tuft Feeder Scanfeed

Web numbers	Fiber composition of webs	Blend ratios (%)
1	Hemp	100
2	PLA	100
3	PP	100
4	Glass fiber	100
5	Glass fiber/PP	33/67

TABLE III
Layering of Fiber Webs for Needle-Punching

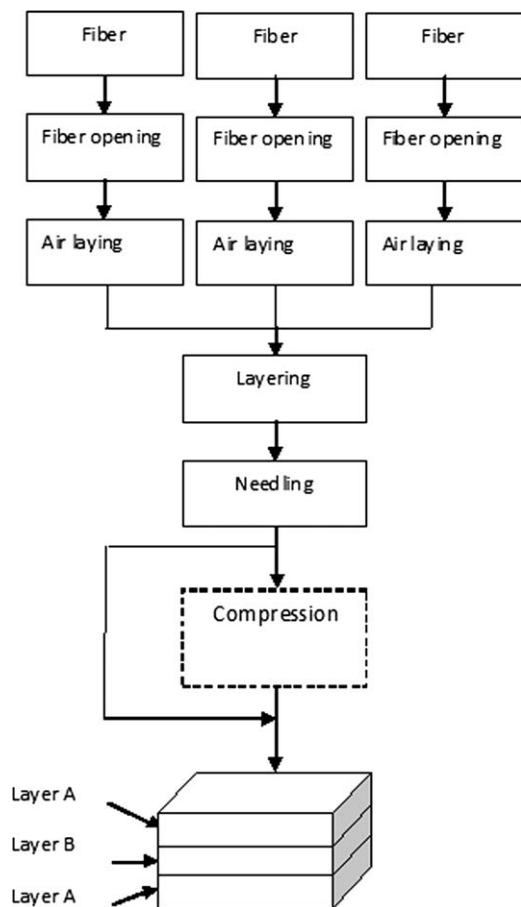| Web number	Web code	Layer 1	Layer 2	Layer 3
1	LHL	PLA	Hemp	PLA
2	PGP	PP	Glassfiber	PP
3	PGI	Glassfiber/PP	Glassfiber/PP	Glassfiber/PP

Figure 1 General production flow chart.

acquire SEM digital images and line scans. At least 30 specimens of hemp fibers and 10 specimens of manmade fibers were measured.

Fabric mass per unit area

Mass per unit area of fabric samples was measured in accordance with ASTM D 3776-07 Standard Test Method for Mass Per Unit Area (Weight) of Fabric.[23] Five samples with a minimum diameter of 8.89 cm (3.5″) were cut and weighed in grams using a Mettler Toledo® Precision Weighing (AG 245) balance.

Thickness

At least five thickness measurements were taken from each sample using an AMES® thickness gauge
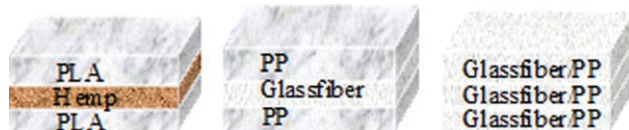

Figure 2 Schematic diagram of web arrangement of LHL, PGP, and PGI, from left to right, in terms of fiber content and layering sequence. [Color figure can be viewed in the online issue, which is available at wileyonlinelibrary.com.]

TABLE IV
Compression Conditions for LHL, PGP, and PGI

Fabric	Pressure (Bar)	Duration (min)			
		7.5	15	30	45
LHL	2.5	X		X	
	5.0		X		X
	7.5	X		X	
	10		X		X
PGP	2.5	X	X	X	X
	5.0	X	X	X	X
	7.5	X	X	X	X
	10	X	X	X	X
PGI	2.5	X	X	X	X
	5.0	X	X	X	X
	7.5	X	X	X	X
	10	X	X	X	X

with a pressure level of 4.14 kPa according to ASTM D 5729-97 Standard Test Method for Thickness of Nonwoven Fabrics.[24]

Compressibility

Thicknesses of the fabrics of each fiber mix were measured before and after compression treatment. The thickness change was measured for all the pressure and duration points in the experimental set up. Compressibility was calculated as the quotient between the absolute strain value and the compression applied.

Porosity

Porosity for five specimens of all nonwoven samples was calculated according to ASTM C 830-00 Standard Test Methods for Apparent Porosity, Liquid Absorption, Apparent Specific Gravity, and Bulk Density of Refractory Shapes by Vacuum Pressure.[25] The standard uses eq. (6):

$$h = 1 - \frac{\rho_w}{\rho_f}, \tag{6}$$

where h is porosity, ρ_w is density of fabric, and ρ_f is the density of the fiber. In this study, PLA fibers had a hollow structure, while all the other fibers were solid. Considering the high aspect ratio of the void in the PLA fiber, the probability of fiber bending, and fiber orienting in directions other than parallel to air flow, the voids in PLA were assumed to be unconnected pores. As only the pores that are interconnected with the ambient air are of interest in terms of sound absorption,[8] the voids in PLA fibers were not included in the porosity. In other words, PLA fibers were assumed to act like solid fibers for sound absorption. Thus, the fiber density was corrected by a factor of void ratio subtracted from unity (1 to 0.18) in the porosity calculation.
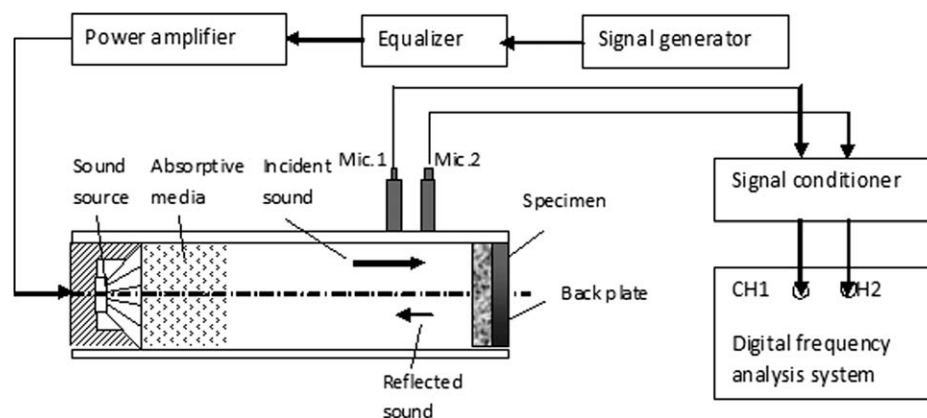
Figure 3 Schematic diagram of acoustical material testing system (adapted from ASTM E 1050-08[28] and Bruel & Kjaer[29]).

Airflow resistivity

Air flow resistivity of nonwoven webs was determined according to ASTM D 737-04 Standard Test Method for Air Permeability of Textile Fabrics.[26] The Frazier® air permeability tester (Frazier Precision Instrument Company) was used. The Frazier® Differential Pressure Air Permeability Instrument gave the rate of flow of air in cubic feet per square foot of sample area per minute, the *Frazier Number*, at a differential pressure of 0.5 in of water.[27] These units were converted to air flow resistivity, r_0, in pascal per second per square meter as shown in eq. (7), where l is the thickness of the fabric in meters (equation derived from Frazier[27] and ASTM D 737-04[26]):

$$r_0 = \frac{0.5 \times 249}{\text{Frazier\_Number} \times 0.00508 \times l}. \qquad (7)$$

Sound absorption coefficient

Normal incident sound absorption coefficient (NAC) was measured according to ASTM E 1050-07 Standard Test Method for Impedance and Absorption of Acoustical Materials using a tube, two microphones, and a digital frequency analysis system.[28] A minimum of three specimens from each sample were tested. A Bruel and Kjaer Pulse™ acoustic material testing system, which included a type 4206 two-microphone impedance tube, a Pulse™ Type 3560 multichannel portable data acquisition unit, and Pulse TM type 7758 software, was used at Carcoustics Tech Center. A 29-mm-diameter tube was used, and the frequency range analyzed was 500 Hz–5 kHz.

A schematic diagram of the acoustical material testing system is given in Figure 3. The impedance tube was composed of a hollow cylinder, a sound source at one end, and a test sample holder at the other. At two locations along the wall of the tube, microphone ports were mounted.

Statistical model building

SAS 8.2 was used for statistical data analysis. Two sets of analyses were carried out according to the dependent variables: namely, air flow resistivity and normal-incidence sound absorption coefficient (NAC). For each dependent variable, two analysis sets have been conducted: one for investigating the effect of material parameters and the other for the investigation of treatment parameters on the dependent variables. A general linear model has been adopted.

RESULTS AND DISCUSSION

A set of models have been generated in this research to analyze the effects of material and treatment factors on air flow resistivity and normal-incidence sound absorption (NAC) performance of the compressed nonwovens. The assumptions for the models are as follows:

1. There has been no structural changes in the fabrics due to compression;
2. The fabrics act uniform throughout their thickness;
3. The fabrics that include fibers of different diameters act as a fabric that includes fibers with a single diameter, which is equal to the weighted average diameter of the constituent fibers;
4. Fibers act as solid fibers.

The evidence for these assumptions was given in Yilmaz et al.,[13] where sound absorptive performance of three-layered needle-punched nonwovens was investigated.

Effect of material parameters on air flow resistivity

As mentioned before, LHL, PGP, and PGI fabrics were compressed under four different pressures for four different durations as shown in Table IV.

TABLE V
Air Flow Resistivity and Structure Parameter Information of Compressed PLA/Hemp/PLA Fabrics, PP/Glassfiber/PP Fabrics, and PP/Glassfiber Intimate Blend Fabrics

Fabric	Basis weight (kg m^{-2}) Mean	σ	Thickness (mm) Mean	σ	Porosity $(1 - \rho_w/\rho_f)$ Mean	σ	Massivity (ρ_w/ρ_f) Mean	σ	Airflow resistivity (10^3 Pa s/m^2) Mean	σ
Compressed PLA/Hemp/PLA fabrics										
Control	1.32	0.08	12.7	0.29	0.91	0.01	0.09	0.01	25.0	3.7
2.5 Bar	1.37	0.06	10.0	0.49	0.88	0.00	0.12	0.00	30.4	1.62
5 Bar	1.30	0.02	8.77	0.76	0.87	0.01	0.13	0.01	35.5	2.73
7.5 Bar	1.49	0.04	9.15	0.86	0.85	0.02	0.15	0.02	34.7	3.18
10 Bar	1.46	0.05	7.91	0.80	0.84	0.01	0.16	0.01	41.2	3.56
Compressed PP/glassfiber/PP fabrics										
Control	1.44	0.13	12.4	0.27	0.90	0.01	0.10	0.01	47.8	4.2
2.5 Bar	1.21	0.12	10.0	0.50	0.90	0.01	0.10	0.01	60.9	13.7
5 Bar	1.36	0.09	9.84	0.35	0.89	0.01	0.11	0.01	78.1	11.9
7.5 Bar	1.31	0.07	9.76	0.46	0.89	0.00	0.11	0.00	76.9	7.78
10 Bar	1.20	0.17	8.96	0.35	0.89	0.01	0.11	0.01	68.6	16.0
Compressed PP/glassfiber intimate blend fabrics										
Control	1.49	0.14	13.1	0.64	0.91	0.01	0.09	0.01	46.1	3.93
2.5 Bar	1.38	0.07	10.7	0.50	0.89	0.00	0.11	0.00	53.1	6.78
5 Bar	1.52	0.08	10.9	0.49	0.88	0.01	0.12	0.01	57.3	5.25
7.5 Bar	1.43	0.12	10.4	0.44	0.89	0.01	0.11	0.01	63.0	8.09
10 Bar	1.50	0.12	10.4	0.53	0.88	0.01	0.12	0.01	61.7	5.08

Table V gives air flow resistivity and material information about LHL, PGP, and PGI fabrics, respectively. As can be seen from Table V, with increasing pressure, the thickness of the fabrics decreases that makes the fabrics denser and more resistant to air flow. With the assumption that there is no structural change, the compression treatment should allow for the investigation of the effect of porosity on air flow resistivity for a broad range of thickness, porosity, and air flow resistivity.

During statistical modeling, all fabrics were assumed to be uniform throughout their thickness. The generated statistical model is given in eq. (8).

$$r_0 = A + B \frac{\rho_W^{1.6}}{\rho_f^{1.6} \times \tilde{a}^2}, \qquad (8)$$

where r_0 is air flow resistivity in mks rayl/m, ρ_w is the density of web, ρ_f is the weighted average density of the fiber in kilogram per cubic meter, and ρ_f

is the weighted root mean square fiber diameter of the fabric in meters, A is 6.372×10^4 kg m^{-3} s^{-1} and B is 7.490×10^{-4} kg m^{-1} s^{-1}. Calculations of weighted average fiber density and diameter were shown previously.[13] The weighted average fiber density and radius information of PGP, PGI, and LHL fabrics are given in Table VI.

When the data points of different materials were plotted individually, as shown in Figure 4(a), it becomes obvious that compressed LHL and PGI followed similar trends, whereas PGP followed a steeper trend with wider scatter. This wide scatter might be caused by the inhomogeneity of the fiber distribution in the 100% glassfiber mid layer due to the tendency of glassfibers to agglomerate in airlaying processing when there is no carrier fiber (PP or PLA for this research). A new model was generated for LHL and PGI fabrics where data points for PGP were eliminated as shown in Figure 4(b). A higher R^2 value, 0.83, was achieved, which provided evidence for the fit of the model given in eq. (9).

TABLE VI
Weighted Average Fiber Diameters and Fiber Densities of PP/Glassfiber/PP layered, PP-Glassfiber Intimate Blend, and PLA/ Hemp/PLA Fabrics

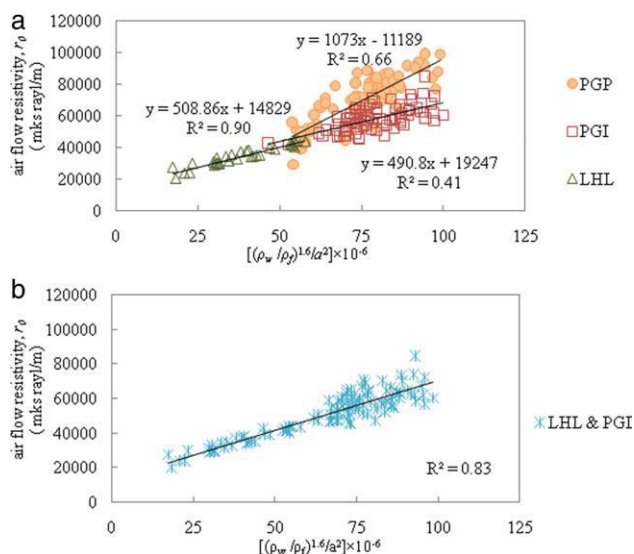| Fabric	Weight fraction of fibers (%) PP	Glass	Number fraction of fibers (%) PP	Glass	Volume fraction of fibers (%) PP	Glass	Fiber radius $\times 10^{-6}$ (m) PP	Glass	Weighted average fiber density $\times 10^{-3}$ (kg m^{-3})	Weighted average fiber radius $\times 10^{-6}$ (m)
PGP	66	34	32	68	85	15	31.5	9.00	1.15	16.3
PGI	66	34	32	68	85	15	31.5	10.9	1.15	17.6
	PLA	Hemp	PLA	Hemp	PLA	Hemp	PLA	Hemp		
LHL	66	34	85	15	25	75	30.9	42.0	1.13	32.8

Figure 4 Comparison of statistical model estimates versus actual values for air flow resistivity values of compressed fabrics. All fabrics are assumed to be uniform through the thickness (a) fabric types are shown separately; (b) data points for LHL and PGI. [Color figure can be viewed in the online issue, which is available at wileyonlinelibrary.com.]

$$r_0 = C + D \frac{\rho_W^{1.6}}{\rho_f^{1.6} \times \tilde{a}^2}, \tag{9}$$

where C is 1.296×10^4 kg m^{-3} s^{-1} and D is 5.750×10^{-4} kg m^{-1} s^{-1}.

In Figure 4(b), the points of LHL and PGI fabrics are plotted. The assumption that fabrics acted as uniform media throughout their thickness was proved to be valid for fabrics other than PGP. Even LHL, which was a sandwiched structure, composed of layers from different materials, acted like a uniform material. The model also shows that the weighted averages for fiber diameter, based on fiber number fraction, and weighted average for fiber density, as calculated in Yilmaz et al.,[13] based on fiber volume fraction, are working successfully for LHL and PGI. This model is very close to the model generated in a former study[13] for mono- and multifiber nonwovens. This suggests that eq. (9) may also be used for monofiber nonwovens. The boundaries suggested for validity of the model, which give the range of the means of material and treatment parameters of the samples of each pressure point as can be seen in Tables V and VI, are a basis weight of 1.30–1.52 kg m^{-2}, fiber diameter of $17.6 \times 10^{-6} - 32.8 \times 10^{-6}$ m, a fabric thickness of $7.9 \times 10^{-3} - 13 \times 10^{-3}$ m, and and a porosity of 0.84–0.91.

An interesting aspect of Figure 4(a) is the relatively low variation in LHL compared to the other fabrics. This aspect becomes even more prominent when the high variation of hemp fibers is taken into account. The low variation in the graph might be

due to the fact that the decrease in the thickness of LHL was greater than those of the other fabrics. This greater change might have reduced the effect of variation in the fabric. The reason for the different trend of PGP was thought to be due to the lack of validity in the assumption that PGP acted as if it was uniform throughout its thickness. This possibility was investigated as the fabrics were studied layer by layer as a composite structure as shown in Figure 5.

The material parameters for individual layers of PGP are given in Table VII. The thicknesses of individual layers were assumed to be the same and one third of the total fabric thickness. The air flow resistance was assumed to be cumulative and was calculated by eq. (10).

$$[r_{0PGP}][l_{PGP}] = [r_{0PP} \quad r_{0GLASS} \quad r_{0PP}] \begin{bmatrix} l_{PGP}/3 \\ l_{PGP}/3 \\ l_{PGP}/3 \end{bmatrix}, \tag{10}$$

$$r = (r_{0PP} + r_{0GLASS} + r_{0PP})l_{PGP}/3$$

$$= \left(\tfrac{2}{3}r_{0PP} + \tfrac{1}{3}r_{0GLASS}\right)l_{PGP}$$

where r_{0PGP}, r_{0PP}, and r_{0GLASS} are air flow resistivity of the nonwoven composite and that of the individual PP and glassfiber layers, respectively, in mks rayl/m, l_{PGP} is the thickness of PGP composite in meters, and r is the specific air flow resistance of the nonwoven composite in mks rayls.

Figure 6 shows the fit of the statistical model with the real data. All fabrics other than PGP were assumed to act as uniform media throughout their thicknesses. PGP was investigated as a multilayer composite material. The decrease in the thickness of all three layers was assumed to be the same. As seen in Figure 6, the slope of PGP is still different from the other fabrics. There has not been any improvement. Other reasons that might be causing this inconsistency were thought to be an uneven decrease in thickness and an uneven mass distribution among layers. The decrease ratio in PP fabric thickness due to compression was measured and found to be 1.3 times greater than that of PGP fabric on average for the same pressure and duration combination.

When the uneven thickness decreases and mass distribution were applied to the model, the fit shown in Figure 7 was achieved. Although, there
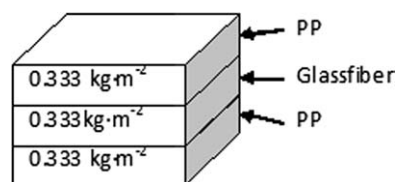

Figure 5 Schematic illustration of PGP.

<div align="center">TABLE VII</div>
<div align="center">Air Flow Resistivity and Structure Parameter Information of Individual Layers of Untreated PGP</div>

Layer	Basis weight (kg m^{-2})		Thickness (mm)		Porosity $(1 - \rho_w/\rho_f)$		Massivity (ρ_w/ρ_f)		$[(\rho_w/\rho_f)^{1.6}/a^2] \times 10^{-6}$	
	Mean	σ	Mean	σ	Mean	σ	Mean	σ	Mean	σ
PP	0.52	0.04	4.14	0.09	0.86	0.01	0.14	0.01	42.8	5.00
Glass	0.52	0.04	4.14	0.09	0.95	0.00	0.05	0.00	104	12.1
PGP	1.57	0.13	12.43	0.27	–	–	–	–	63.2	7.33

was some enhancement, such as the intercept of the curve of PGP becomes similar to the other fabrics, there was still a difference in the slopes. This might be due to extra reflectivity between PP and glass-fiber layers. This situation suggested that there was a greater difference between the air flow resistivity of PP and glassfiber layers compared to the difference between those of PLA and Hemp layers in LHL fabric or between individual layers of PGI. This finding was supported by the fact that the difference between the average diameters of PP and glassfiber was much more than that between the PLA and hemp layers, which have relatively similar fiber diameters. More research is needed to model the air flow resistivity behavior of composites, which consist of layers with substantially different material parameters.

Effect of treatment parameters on air flow resistivity

The reason for analyzing the effect of compression-treatment parameters was to be able to predict the change in the air flow resistivity of the materials when the material parameters of the starting fabric and the compression-treatment parameters were known.

The main effect of compression was on thickness change, and the fabrics showed different thickness

decreases for the same treatment conditions. To explain these differences, a compressibility variable was used. In the current research, compressibility was calculated by the following equation:

$$c_m = \frac{\left| \Delta l / l_i \right|}{p}, \tag{11}$$

where c_m is compressibility in pascal^{-1}, Δl is the change in thickness in mm, l_i is initial thickness in millimeter, and p is pressure in pascal. Thicknesses of LHL, PGP, and PGI fabrics were measured before and after compression treatment. Strain values of the fabrics were calculated for each pressure point—duration combination in the experimental set-up. Effect of duration has not been included in the model.

The stress–strain behaviors of the fabrics are shown in Figure 8. The compressibility was determined as the quotient between the absolute strain and the compression pressure applied. It should be noted that in Figure 8, the pressure is shown in Bars; however, in compressibility, the pressure is taken in pascals. The differences between compressibility values among different samples were found to be statistically significant, in spite of the high variation. The greatest thickness change was experienced in LHL, followed by PGP and PGI. The differences
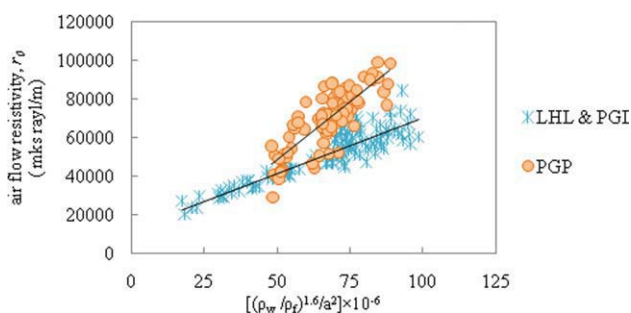

Figure 6 Comparison of statistical model estimates versus actual values for air flow resistivity values of single-fiber webs and compressed fabrics. PGP is investigated as a multilayer composite, which has layers of equal thickness. All other fabrics are assumed to be uniform through the thickness. PGP and the other data points are shown separately. [Color figure can be viewed in the online issue, which is available at wileyonlinelibrary.com.]
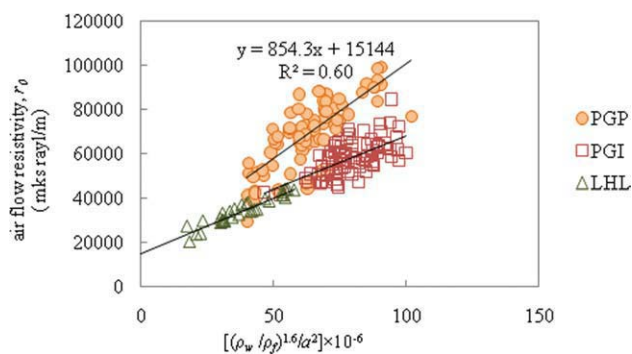

Figure 7 Comparison of statistical model estimates versus actual values for air flow resistivity values of compressed fabrics. PGP is investigated as a multilayer composite. Uneven thickness decrease and mass distribution among layers are applied. LHL and PGI fabrics are assumed to be uniform through the thickness. [Color figure can be viewed in the online issue, which is available at wileyonlinelibrary.com.]
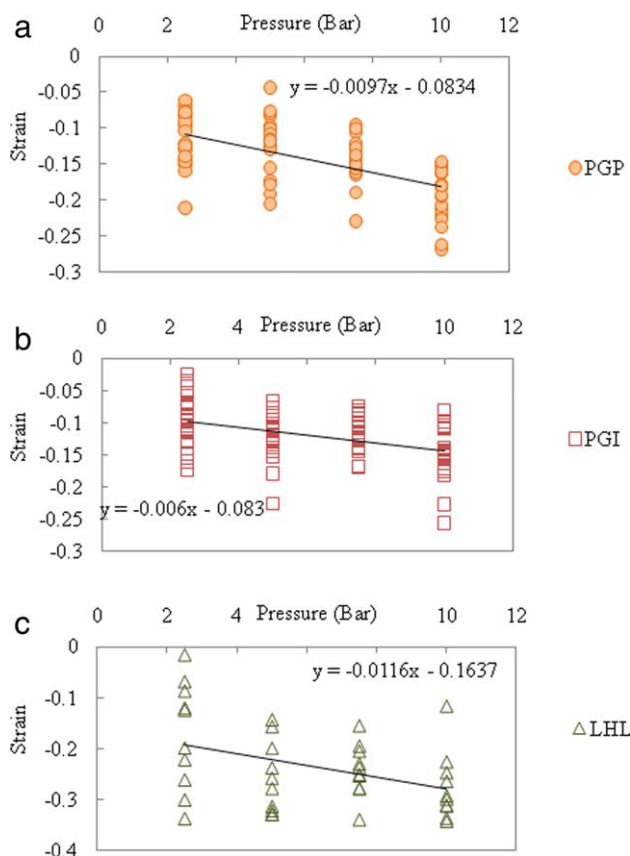
Figure 8 Stress–strain plots of the compressed fabrics. (a) PP/glass fiber/PP-layered fabrics; (b) PP-glassfiber intimate blend; (c) PLA/Hemp/PLA-layered fabrics. [Color figure can be viewed in the online issue, which is available at wileyonlinelibrary.com.]

between the structures of PGP and PGI, which contained the same fiber types, were in the placement of fibers and in the glassfiber diameters. In PGI, the fibers were intimately mixed in each layer, whereas, in PGP, each layer was composed of one fiber type. In PGP, the glassfiber diameter was 20% smaller than the same fiber type, which is used in PGI. The coarser glassfiber in PGI might have more resistance to compression compared to that in PGP. Intimate blending might also have an effect on compressibility.

The goal in treatment effect analysis was to use as few material parameters as possible. The first model included the variables of pressure and compressibility as shown in Figure 9(a). The y-axis in Figure 9 shows the ratio of the normalized air flow resistivity values of the treated fabric to that of the untreated one. The normalization was calculated according to the following equation:

$$r_{0n} = \frac{r_0}{w^{1.6}}, \tag{12}$$

where r_{0n} is the normalized air flow resistivity in $kg^{-0.6}$ $m^{0.2}$ s^{-1}, r_0 is air flow resistivity rayl m^{-1}, and

w is the basis weight of the fabric in kilogram per square meter.

In Figure 9(a), it is obvious that pressure has a positive effect on air flow resistivity. The higher the pressure and the decrease in the thickness, the lower is the porosity, that is, the fraction of pores through which air can flow. Duration was not found to be a significant factor. This might be due to the narrow range of duration (7.5–45 min). A broader range of durations might be studied for future research. The
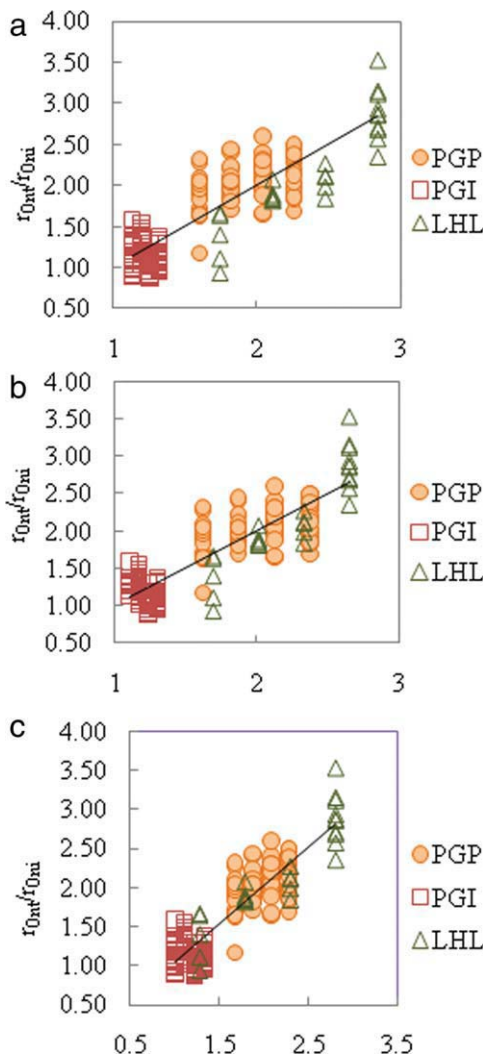

Figure 9 Comparison of statistical model estimates versus actual values for air flow resistivity values of compressed fabrics. (a) X-axis is a function of pressure and pressure-compressibility interaction. [$x = 1.38 - 0.21p + 30.6$ pcm]. p is pressure in Bar, cm is compressibility in Bar^{-1}. (b) X-axis is a function of pressure and pressure-compressibility interaction. [$x = 1.37 + 0.21$ p $+ 6.70 \times 10^{-5}$ p $cm^{-1.6}$]. p is pressure in Bar, cm is compressibility in Bar^{-1}. (c) X-axis is a function of pressure, compressibility, fiber size, and fiber density according to eq. (13). p is pressure in Bar, cm is compressibility in Bar^{-1}, a is fiber diameter in μm, and ρf is weighted average fiber density. [Color figure can be viewed in the online issue, which is available at wileyonlinelibrary.com.]

R^2 obtained was 0.76, which might be considered reasonable for materials with such inherent variability. However, when each material type in Figure 9(a) was separately observed, it was seen that LHL gave values lower than the curve. This meant that more variables were needed to explain the air flow resistivity behavior of compressed fabrics.

To improve the fit, minus 1.6th power of compressibility was used to be consistent with the fact that air flow resistivity was normalized by gsm to the 1.6th power. The findings were plotted in Figure 9(b). Although there was a slight improvement, data points of LHL were still well below the curve, which necessitates more variables to be included in the model.

To improve the model, two more material parameters were included: weighted average fiber size and fiber density. It is known that air flow resistivity strongly depends on the fineness of the fiber. The fiber diameter was added to the model to explain this effect. Fiber density to the 1.6th power was also added to the model to include the effect of fabric porosity, as air flow resistivity was normalized by gsm to the 1.6th power.

As seen from Figure 9(c), although there is only one point increase in R^2 value to 0.78, the fit of LHL has improved substantially. Therefore, with the following equation, it is possible to predict the air flow resistivity of the compressed material, given the properties of the untreated material and the pressure applied.

$$r_{0nt}/r_{0ni} = 3.2 \times 10^{-1} + \frac{E}{\rho_f^{1.6} a^2} + Fp + \frac{G}{c_m^{1.6}} p - \frac{H}{\rho_f^{1.6} a^2 c_m^{1.6}} p, \tag{13}$$

where r_{0nt} is the air flow resistivity normalized by $[\text{gsm } 10^{-3}]^{1.6}$ of the compression-treated fabric, r_{0ni} is the air flow resistivity normalized by $[\text{gsm } 10^{-3}]^{1.6}$ of the untreated fabric, p is pressure in pascal, c_m is compressibility in pascal^{-1}, a' is fiber diameter in meter, and ρ_f is fiber density in kilogram per cubic meter. The coefficient E is $3.76 \times 10^{-5} \text{ kg}^{1.6} \text{ m}^{-2.8}$, F is $2 \times 10^{-6}/\text{pascal}$, G is $5.0 \times 10^{-18} \text{ kg}^{-2.6} \text{ m}^{2.6} \text{ s}^{5.2}$, and H is $3.97 \times 10^{-22} \text{ kg}^{-1} \text{ m}^{-0.2} \text{ s}^{5.2}$. The boundaries suggested for validity are a basis weight of 1.20–1.52 kg m^{-2}, fiber diameter of $16.3 \times 10^{-6} - 32.8 \times 10^{-6}$ m, a fabric thickness of $7.9 \times 10^{-3} - 13 \times 10^{-3}$ m, a pressure of 2.5–10 Bars, and a porosity of 0.84–0.91.

Effect of material parameters on normal-incidence sound absorption coefficient

In Figure 10, the average NAC values of compressed fabrics are shown. Compression decreased the sound absorption coefficient values as expected. After compression, the thickness, which is a very important parameter for sound absorption, decreased as mentioned before. The greatest decrease was experienced for LHL fabrics, which might be due to the greater thickness change in LHL fabrics.
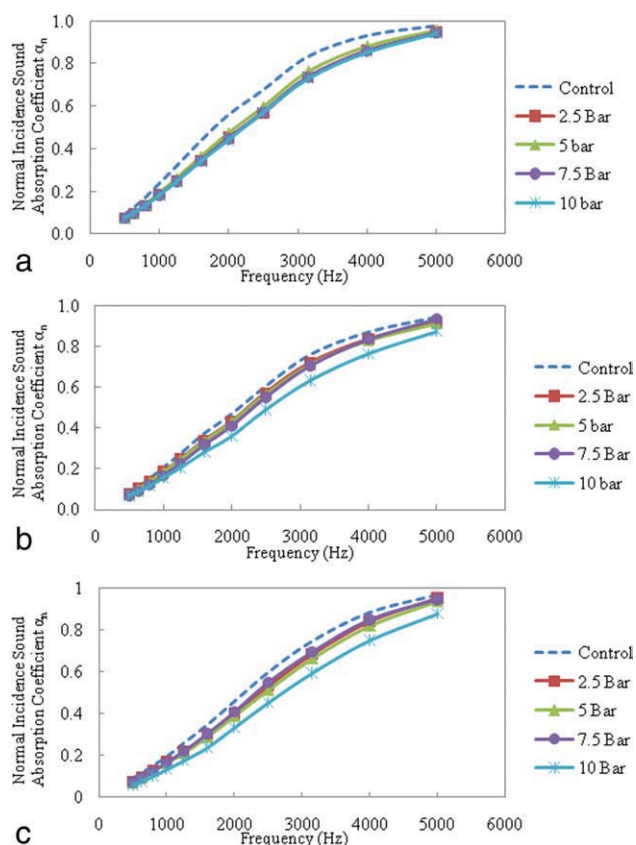
Figure 10 Average normal-incidence sound absorption on fabrics treated under different pressures. (a) PGP, (b) PGI, and (c) LHL. [Color figure can be viewed in the online issue, which is available at wileyonlinelibrary.com.]

The model given in eq. (14) was generated with the variables of frequency, air flow resistivity, and thickness.

$$\alpha_n = \sin\left(-5.56 \times 10^{-1} + If + Jr_0 + Kl\right), \tag{14}$$

where α_n is the normal-incidence sound absorption coefficient (NAC), f is frequency in Hertz, r_o is air flow resistivity in mks rayl/m, I is $2.61 \times 10^{-4} \text{ Hz}^{-1}$, J is $1.06 \times 10^{-6} \text{ kg}^{-1} \text{ m}^3 \text{ s}$, and K is $4.11 \times 10^{-5} \text{ m}^{-1}$. A very high coefficient of determination, R^2, of 0.97 is achieved. The comparison of the model estimates and the real data points are given in Figure 11. As seen from Figure 11, all three fabrics agree well with the model. The boundaries suggested for validity are a basis weight of 1.20–1.52 kg m^{-2}, fiber diameter of $16.3 \times 10^{-6} - 32.8 \times 10^{-6}$ m, a fabric thickness of $7.9 \times 10^{-3} - 13 \times 10^{-3}$ m, porosity of 0.84–0.91, air flow resistivity of $25.0 - 78.1 \times 10^3$ mks rayl/m, and a frequency range of 500 Hz–5 kHz.

Effect of treatment parameters on normal-incidence sound absorption coefficient

Among compression-treatment parameters, pressure was found to be the significant factor affecting NAC.

To explain the different behaviors of fabrics under compression, the compressibility, c_m, as calculated in eq. (11), was included in the model. To reflect the difference in the structures of the starting materials, fiber diameter, a, and fiber density, ρ_f, were included in the model, along with the compressibility. This model is given in eq. (15) as shown below. To be consistent with the normalization of air flow resistivity, $\sin^{-1}(\alpha_n)$ was normalized by $[\text{gsm} \times 10^{-3}]^{1.6}$. An R^2 of 0.97 was achieved. Figure 12 gives the comparison of the model estimates and the real data points. As seen from the figure, all three of the fabrics agreed well with the model.

$$\alpha_n = \sin\left[\left(-5.56 \times 10^{-2} + Lf - Mp - \frac{N}{c_m^{1.6}}p + \frac{O}{a^2\rho_f^{1.6}}\right) \right.$$
$$\left. \times P\,gsm^{1.6}\right], \quad (15)$$

where L is 1.58×10^{-4} Hz^{-1}, M is 2×10^{-8} kg^{-1} m s^2, N is 1×10^{-19} kg$^{-2.6}$ m$^{2.6}$ s$^{5.2}$, O is 1.43×10^{-6} kg$^{1.6}$ m$^{-2.8}$, and P is $1 \times 10^{-4.8}$ kg$^{-1.6}$ m$^{3.2}$. The boundaries for validity are a basis weight of 1.20–1.52 kg m^{-2}, fiber diameter of $16.3 \times 10^{-6} - 32.8 \times 10^{-6}$ m, a fabric thickness of $7.9 \times 10^{-3} - 13 \times 10^{-3}$ m, porosity of 0.84–0.91, air flow resistivity of $25.0 \times 10^3 - 78.1 \times 10^3$ mks rayl/m, and a frequency range of 500 Hz–5 kHz.

CONCLUSIONS

The effects of material and treatment parameters on airflow resistivity and normal-incidence sound absorption coefficient of compressed nonwoven composites made up of three layers were studied. The material parameters included fiber diameter and fabric porosity. The treatment factors included the applied pressure and duration of compression. The three-layered nonwoven composites can be classified based on the material content and fiber blend. LHL and PGP were sandwich structures consisting of PLA/Hemp/PLA and PP/glassfiber/PP layers,
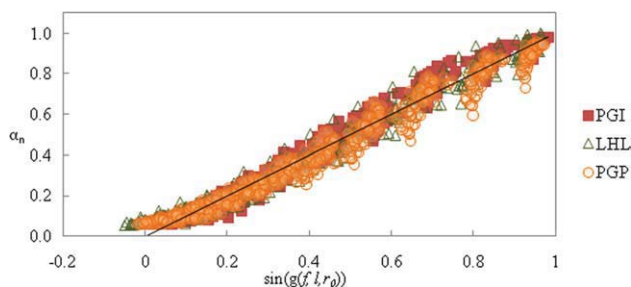

Figure 12 Comparison of statistical model estimates versus actual values for NAC of compressed fabrics. X-axis is a function of frequency, pressure, compressibility, fiber diameter, fiber density, and gsm. [Color figure can be viewed in the online issue, which is available at wileyonlinelibrary.com.]

respectively. PGI consisted of three layers of PP-glassfiber intimately blended together. Statistical models were developed to predict air flow resistivity from material parameters and the change in air flow resistivity due to compression-treatment parameters. The independent variables of the former model were porosity and fiber size, and those of the latter were compressibility, pressure, and initial material parameters. An increase in air flow resistivity was found due to compression.

Two statistical models were developed for the prediction of sound absorption coefficient based on material and treatment parameters. The independent variables of the first model were air flow resistivity, thickness and frequency, and those of the latter were compressibility, pressure, frequency, and initial material parameters. No significant effect of compression duration was detected on air flow resistivity or sound absorption. With the models generated, it is possible to predict the air flow resistivity and sound absorption coefficient of compressed fabrics once the initial material parameters and compression conditions are known.

Figure 11 Comparison of statistical model estimates versus actual values for NAC of compressed fabrics. X-axis is a function of frequency, thickness, and air flow resistivity. [Color figure can be viewed in the online issue, which is available at wileyonlinelibrary.com.]
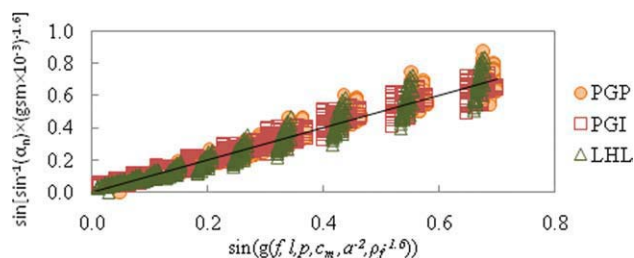
References

1. Zhou, H.; Li, B.; Huang, G. J Appl Polym Sci 2006, 101, 2605.
2. Yilmaz, N. D. Acoustic properties of biodegradable nonwovens, Ph.D Thesis, North Carolina State University, North Carolina, 2009.
3. Kuttruff, H. Acoustics: An Introduction; Taylor & Francis: New York, 2007.
4. Ng, Y.-H.; Hong, L. J Appl Polym Sci 2006, 102, 1202.
5. Fahy, F. Foundations of Engineering Acoustics; Academic Press: San Diego, CA, 2001.
6. Cox, T. J.; D'antonio, P. Acoustic Absorbers and Diffusers; Taylor & Francis: New York, 2004.

7. Yilmaz, N. D.; Banks-Lee, P.; Powell, N. B. INTC 2008 International Nonwovens Technical Conference Proceedings, TX, USA, 2008.

8. McRae, J. D.; Naguib, H. E.; Atalla, N. J Appl Polym Sci 2010, 116, 1106.

9. Ingard, K. U. Notes on Sound Absorption Technology; Noise Control Foundation: Poughkeepsie, NY, 1994.

10. Banks-Lee, P.; Peng, H.; Diggs, L. Joint INDA-TAPPI Conference: International Nonwovens Technical Conference Proceedings, Association of Nonwoven Fabrics Industry, USA, 1992; p 209.

11. Delany, M. E.; Bazley, E. N. Appl Acoust 1970, 3, 105.

12. Mechel, F. P. Formulas of Acoustics; Springer: Berlin, Germany, 2002.

13. Yilmaz, N. D.; Banks-Lee, P.; Powell, N. J.; Michielsen, S. J Appl Polym Sci 2011, 121, 3056.

14. American Society for Testing and Materials, ASTM C 522–03 Standard Test Method for Airflow Resistance of Acoustical Materials, 2008.

15. Wang, X. Y.; Gong, R. H. J Appl Polym Sci 2006, 102, 2264.

16. Vitchuli, N.; Shi, Q.; Nowak, J.; McCord, M.; Bourham, M.; Zhang, X. J Appl Polym Sci 2011, 116, 2181.

17. Kan, C. W. J Appl Polym Sci 2008, 107, 1584.

18. Mohammadi, M. Heat barrier properties of heterogeneous nonwoven materials, Ph.D Thesis, North Carolina State University, North Carolina, 1998.

19. Kan, C. W.; Yuen, W. M. J Appl Polym Sci 2006, 102, 5958.

20. Castagnède, B.; Aknine, A.; Brouard, B.; Tarnow, V. Appl Acoust 2000, 61, 173.

21. Jayaraman, K. A.; Banks-Lee, P.; Jones, M. Joint INDA-TAPPI Conference—INTC 2005: International Nonwovens Technical Conference Proceedings, Association of Nonwoven Fabrics Industry, MO, USA, 2005; p 403.

22. American Society for Testing and Materials, ASTM D 1577 07 Standard Test Methods for Linear Density of Textile Fibers, 2007.

23. American Society for Testing and Materials, ASTM D 3776 07 Standard Test Methods for Mass Per Unit Area (Weight) of Fabric, 2007.

24. American Society for Testing and Materials, ASTM D 5729–97 Standard Test Method for Thickness of Nonwoven Fabrics, 1997.

25. American Society for Testing and Materials, ASTM C 830–00 Standard Test Methods for Apparent Porosity, Liquid Absorption, Apparent Specific Gravity, and Bulk Density of Refractory Shapes by Vacuum Pressure, 2000.

26. American Society for Testing and Materials, ASTM D 737–04 Standard Test Method for Air Permeability of Textile Fabrics, 2004.

27. Frazier Precision Instrument Company, Inc., Frequently asked questions about the Frazier differential pressure air permeability instrument 2009, http://www.frazierinstrument.com/products/fap/fap-faq.html (Accessed December 3, 2009).

28. American Society for Testing and Materials, ASTM E 1050–07 Standard Test Method for Impedance and Absorption of Acoustical Materials Using a Tube, Two Microphones and a Digital Frequency Analysis System, 2007.

29. Bruel & Kjaer, Product data impedance tube kit (50 Hz-6.4 kHz)- type 4206 2009 http://www.bksv.com/doc/Bp1039.pdf (accessed December 3, 2009).